Available online at www.sciencedirect.com

ScienceDirect

Procedia Structural Integrity 6 (2017) 56–63

Structural Integrity Procedia

www.elsevier.com/locate/procedia

XXVII International Conference "Mathematical and Computer Simulations in Mechanics of Solids and Structures". Fundamentals of Static and Dynamic Fracture (MCM 2017)

Stress Concentrations in Composites with Microvascular Channels

Hamed Tanabi[a]*,Ahmed Al Shawk[b], Baris Sabuncuoglu[c]

[a]*Mechanical Engineering Department, University of Turkish Aeronautical Association, Ankara, Turkey*
[b]*Graduate School of Natural and Applied Sciences, University of Turkish Aeronautical Association, Ankara, Turkey*
[c]*Mechatronic Engineering Department, University of Turkish Aeronautical Association, Ankara, Turkey*

Abstract

Microvascular channels in fiber-reinforced composites offer various functionalities ranging from self-healing and damage monitoring, to active thermal management. However, the tradeoff between extended functionalities and mechanical performance at vascularized composites is still an issue. In this study, a three dimensional finite element model is developed to investigate the stress concentrations generated around macro-vascular channels for various channel configurations and lamination sequences. Results indicate that the stress distribution around vascular channel is same for symmetric stacking configurations spite of having different layer just above the channel and different resin pocket dimensions. The effect of changing the vascule diameter is mostly observed in UD 0 configuration.

Peer-review under responsibility of the MCM 2017 organizers.

Keywords: Finite element; vascular channel; fiber reinforced composites

1. Introduction

Introduction of microvascular channels embedded within fiber reinforced composites offers the potential for significant developments in functionality. For instance, these channels can be used for thermal management and active cooling of composite laminates (Aragón et al., 2007; Kozola et al., 2010). Patrick *et al.* (Patrick et al., 2014)

* Corresponding author. Tel.:+90-553-222-3813; fax: +90-312-342-8460.
E-mail address: htanabi@thk.edu.tr

Peer-review under responsibility of the MCM 2017 organizers.
10.1016/j.prostr.2017.11.009

and Norris *et al.* (Christopher J. Norris et al., 2011) conducted in situ self-healing in fiber reinforced composites using microvascular networks. While providing these functions, the microvascular channels also introduce a modification in the structure of the composites. The effect of micro channels on the structural behaviour of composites is investigated experimentally and numerically in quite a few studies. The studies on tensile and compressive properties of vascularized composites show that the loss of elastic moduli is negligible when size of micro channel is less than a critical diameter (Coppola et al., 2014; Kousourakis et al., 2008). However, the modulus of elasticity decreased with channel diameters greater than a threshold. Also it was reported that the loss in modulus was much greater for the case at which channels are in the transverse direction. The reported results in (Jensen et al., 1992a, 1992b; Zhou et al., 2004) show 2% - 9% decrease in the in-plane strength of vascularized composites when a certain vascular diameter is reached. In (Trask and Bond, 2006), authors reported a 16% reduction in compressive strength of a carbon/epoxy composite laminate containing 0.6 mm diameter channel and a small reduction in flexural strength of the composite laminate with the same vascular diameter. Parallel to the experimental studies, very few studies have focused on the numerical modelling methods to investigate the mechanical behaviour of composites employing micro-vascular channels. Huang et al. (Huang et al., 2010) performed finite element analysis (FEA) using a plain strain model to study the crack initiation and compression strength in vascularized composites under transverse loading. This model was used by (Nguyen and Orifici, 2012) for a damage analysis. They (Nguyen and Orifici, 2012) studied the effect of the channel spacing and laminate thickness on the failure behaviour under various loading conditions. The reported results in (Nguyen and Orifici, 2012)show that, the channel orientation respect to the fiber direction does not have noticeable effect on the strength of the composite laminate under combined load. Surveying the available literature related to microvascular channels shows that except the study by (Huang et al., 2010), none of the computational studies investigated the stress concentrations which can explain the stress re-distribution and failure behaviors due to exist of micro channels. In (Huang et al., 2010), results for only a specific channel and composite stacking configuration is given. In addition, only transverse loading is considered. In this work, stress concentrations generated around microvascular channels for various channel configurations are investigated and compared with each other by a three dimensional finite element model under tensile load. Furthermore, this study considers one of the issues that have never been considered in the previous studies: the effect of lamination sequence on the stress concentrations.

2. Sample preparation

In this study, Vaporization of Sacrificial Components (VaSCs), was introduced by (Esser-kahn et al., 2011), is used to create hollow micro channels in continuous glass fiber reinforced composites. In this process, unidirectional glass fabrics are laid inside the mold together with a catalyst-saturated polylactic acid (PLA) sacrificial filament. Then fabrics are impregnated with a low - viscosity resin using Vacuum Assisted Resin Transfer Molding (VARTM). Composites were cured in an oven at 80 ºC for one hour then at 160 ºC for 4 hours. Following the cure, composite plates were trimmed around the edges and then samples are put in a vacuum oven at 200 ºC for 24 hours to vaporize the sacrificial component (PLA filament).

In the present case, glass fiber reinforced composites are prepared with a fiber volume fraction of 55% containing vascular channel of 1 mm diameter along the laminate mid-plane. The fabricated laminates contain 16 plies with stacking orders $[90/0]_{4s}$ or $[0/90]_{4s}$.

3. Finite Element Model

3.1. Geometrical Configuration

Micro scale images are taken from cross section of the vascularized laminates. These images are then used to extract the dimensions of the model (Fig. 1). As it is seen in Fig. 1, there is a resin-rich region around vascular channel. Also, it was found that there is a significant geometrical difference in the resin-rich region between [90/0] and [0/90] stacking orders. The resin-rich pocket in [0/90] is much larger than the one in [90/0]. These dimensional differences are also confirmed by the reported results with (Nguyen and Orifici, 2012; C J Norris et al., 2011). The

dimensions obtained via these images are shown in Table 1 as bold letters along with the dimensions of the case studies considered in this study. Note that for vascule diameters smaller than 1 mm dimensions are scaled. In order to investigate the effect of plies stacking sequence more deeply, UD 0 and UD 90 configurations were modeled as well in addition to [90/0] and [0/90] configurations.

Note that only one quarter of the real specimen section is modeled due to the symmetry. Also the length of the model is equal to 25mm scaled by 1:10 of the real specimen. Continuum shell elements were chosen specific to the FE code ABAQUS® to model the composite laminates and the rest of the model is meshed with 8-noded linear 3D elements. The regions of interest had the finer mesh and it is located around the channel (the resin pocket and the curved layers). Symmetry boundary conditions are applied at x-z and y-z planes where the channel exists.

3.1. Materials and Properties

The properties of the composite are determined from the fiber and matrix properties taken from the supplier's data using rule of mixtures (Table 2). Here "1" direction shows the fiber direction whereas "2 and 3" directions show the transverse directions. The rotation of the directions according to stacking direction is taken into account in the "*section assignments*" part in the graphical user interface of ABAQUS.

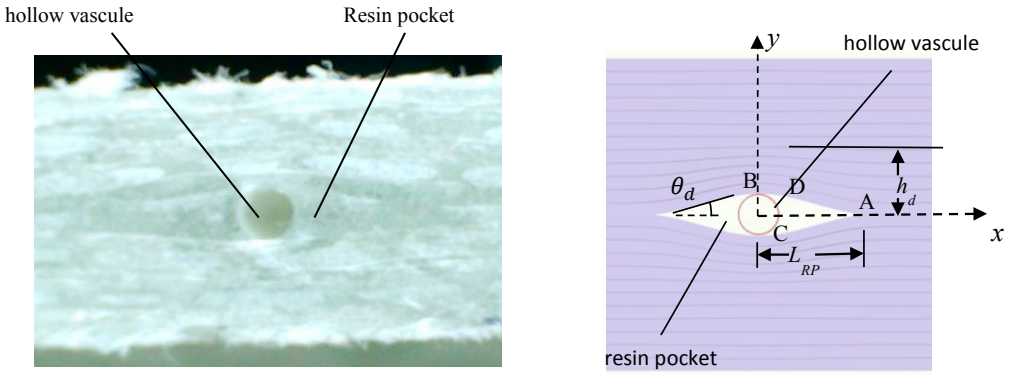

Fig. 1. (a) Micro-pictures for sample embedded with vascule diameter of 1mm, $[0/90]_{4s}$, (b) Geometrical parameters

Table 1. Geometric parameters of vascules for the present samples

Vascule diameter (mm)	Resin-rich pocket length (mm) (L_{RP})	disturbance height (mm) (h_d)	fiber disturbance angle (θ_d)	lay-up system
1	**3.274**	**1.461**	**10°**	**$[0/90]_{4s}$**
0.8	2.593	1.4437	9°	$[0/90]_{4s}$
0.6	2.139	1.15875	8°	$[0/90]_{4s}$
0.4	1.56877	0.8756	8°	$[0/90]_{4s}$
1	**1.8**	**0.95**	**16°**	**$[90/0]_{4s}$**
0.8	1.269	0.684	18°	$[90/0]_{4s}$
0.6	0.856	0.462	20.4°	$[90/0]_{4s}$
0.4	0.514	0.277	23°	$[90/0]_{4s}$

Table 2. Material properties for E-Glass/Ardur-564: Araldite 2954 unidirectional lamina for v_f = 55%

		Young's Modulus (GPa)		Shear Modulus (GPa)		Poisson's Ratio
E-Glass fiber [26]		73.35				0.22
Araldite 564: Aradur2954 (Hunstman LLC)		2.5				0.35
Composite laminate	E_{11}	40.917	G_{12}	1.982	υ_{12}	0.2785
	E_{22}	5.33	G_{23}	1.942	υ_{23}	0.37
	E_{33}	5.33	G_{13}	1.932	υ_{13}	0.2785

3.2. Boundary Conditions, Loading and Meshing

The boundary conditions are shown in Fig. 2. The model is divided into 3 sub-sections. The first section is the fixed grip which has a length equal to one fifth of the whole model length, and fixed in all directions. The second section is the zone between the grips. The third section is the moving grip with length equal to the fixed grip, a displacement boundary condition in the z-direction is applied to this grip to give a 0.1% strain as this is accomplished by multiplying the strain with the distance between the grips.

4. Results

4.1. Effect of Stacking Configuration

Fig. 3 shows the stress concentrations (σ/σ_0) along two paths for various stacking configurations. Here, z-direction is the tensile direction, x-direction is the transverse direction and y is the stacking direction. The normalized stresses (σ_o) are calculated by summing up the reaction forces in each node at the fixed grip dividing by the cross-sectional area of the model. According to Fig. 3, the highest normalized stresses are observed in UD 90 configuration whereas lowest ones were observed for UD 0 configuration. In another words, resin-rich pocket carries more longitudinal force when the laminate is UD 90 compared to the other stacking configurations. Thus, the effect of stress concentrations is more pronounced for this configuration. Since UD 0 has the highest stiffness, most of the load is carried by the laminate rather than the resin rich region. For this reason, the tensile stress concentrations on the resin region are the lowest.

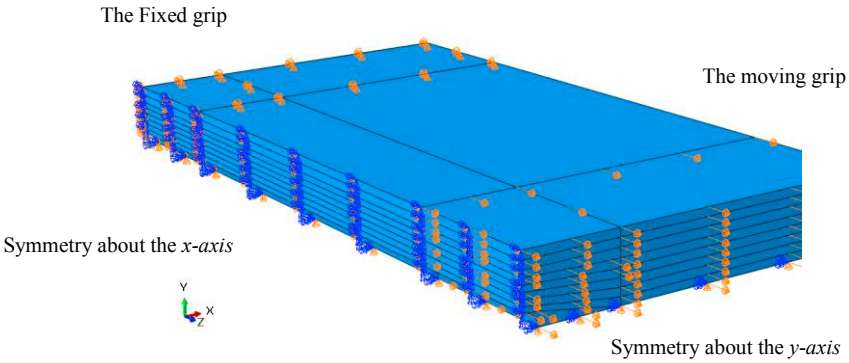

Fig. 2. Boundary conditions of the FEA model

As expected, the results of the models with $[0/90]_{4s}$ and $[90/0]_{4s}$ are somewhere between the results obtained for UD 0 and UD 90 stacking configurations. Considering the presented results at Fig. 3, it can be seen that the normalized stress for $[0/90]_{4s}$ and $[90/0]_{4s}$ are almost the same even though the plies stranding the resin pocket and the dimensions of the resin pocket are different. This is an interesting result as this shows the choice of the lamina stacking order is not effective on the stress distributions near vascular channel under this type of loading.

Fig. 4 presents the stress distribution contours for 1 mm diameter of vascular channel with various stacking sequences. It is observed that the stresses are more concentrated close to the vascular region in UD 90 model whereas a more homogeneous distribution is seen in UD 0 model. The $[0/90]_{4s}$, and $[90/0]_{4s}$ results lie somewhere between these two extremes.

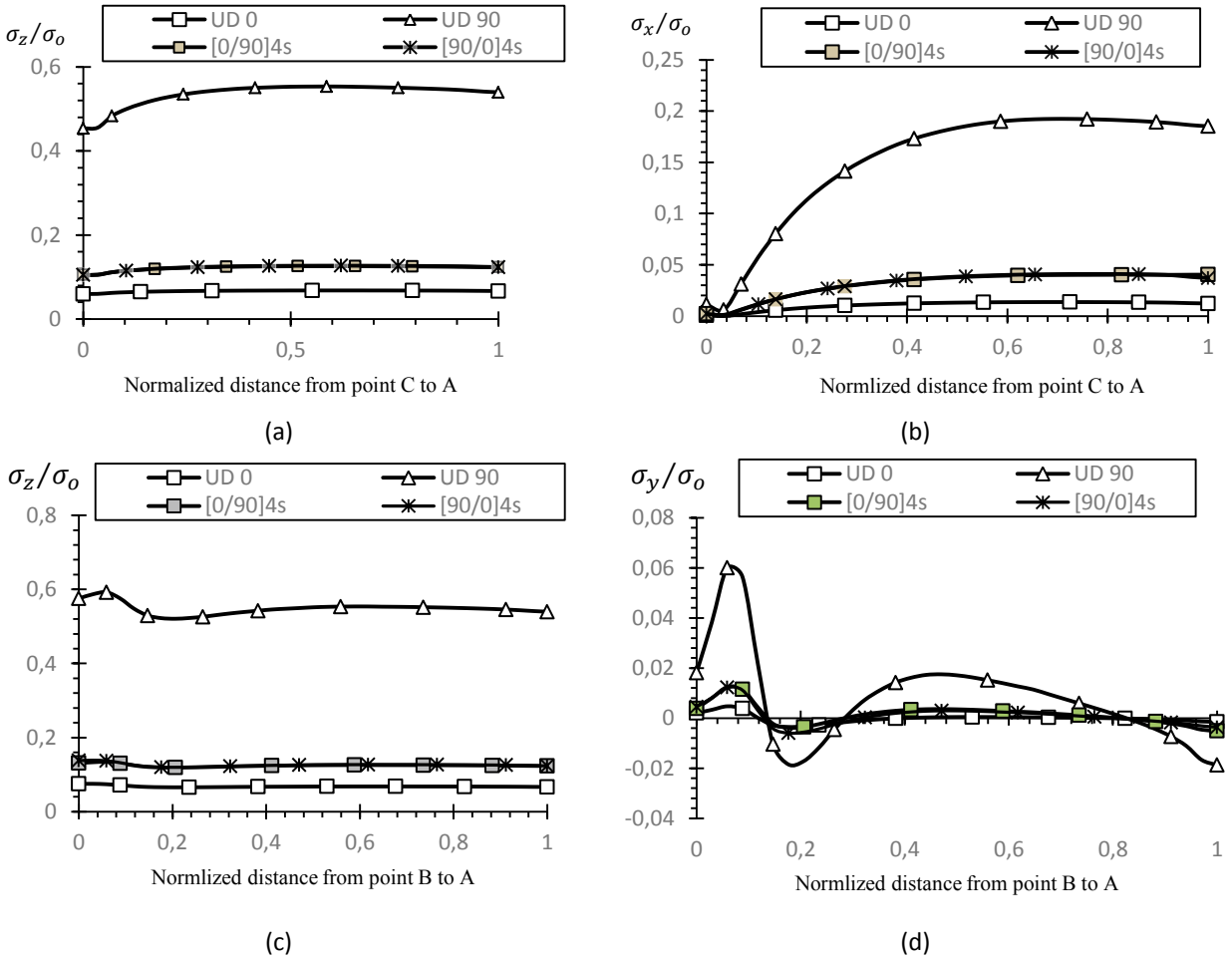

Fig. 3. (a) Normalized σ_z ; (b) Normalized σ_x distribution along the normalized distance C-A; (c) Normalized σ_z ; (d) Normalized σ_y distribution along the normalized distance B-A for the sample with 1 mm diameter microvascular channel.

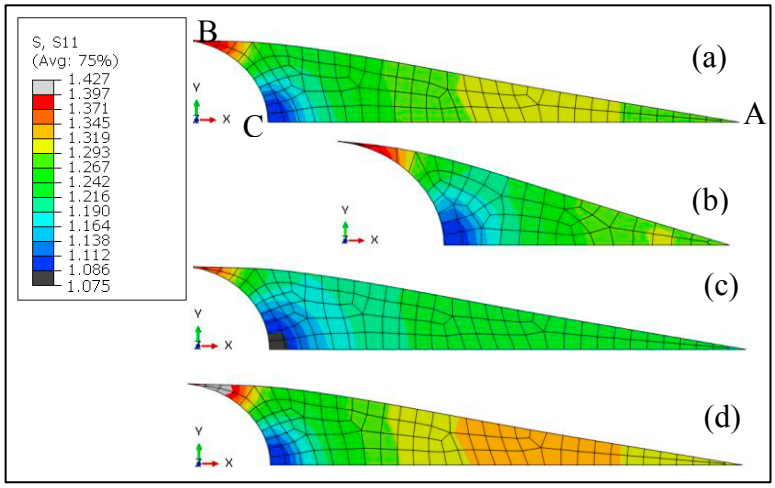

Fig. 4. Longitudinal stress distribution above the resin-rich pocket: (a) $[0/90]_{4s}$; (b) $[90/0]_{4s}$; (c) $[0]_{16}$; and (d) $[90]_{16}$

4.2. Effect of channel size

Fig. 5 illustrates the distribution of the normalized stress in resin reach zone for UD0 and UD90 configurations at various vascular channel diameters. These graphs show the same tendency along the resin pocket. The magnitudes of stresses are almost equal at point C and gets larger for larger channel diameters. This means that the stresses are more concentrated when the channel diameter is larger whereas a better distribution of stresses is observed for lower vascular channel diameters. Furthermore the location of the maximum stress is shifted away from the center as the channel size is increased

Considering the simulation results for various stacking sequences and different channel diameters, the maximum normal stress for each case is obtained and presented in Table 3. When different stacking sequences are compared with each other, the variations in maximum normalized stress at various vascular channel diameters are slightly higher in UD 0 compared to the other stacking configurations although the values are lower. Thus, it can be concluded that UD 0 laminates are more sensitive to the change in the vascular channel diameter than the other configurations. The small variations in the results cannot be attributed to numerical error as exactly the same models are used for the same vascular channel diameter and only the stacking direction is changed.

The stress contours in the resin-rich pocket for $[0/90]_{4s}$ stacking order are depicted in Fig. 2. The longitudinal stress near point C is lower compared to the one at point B (top of the vascule). A larger high stress area can be observed in the case of vascule diameter 1 mm compared to the ones with smaller diameters. This clearly reveals the effect of diameter in the stress distributions. Larger vascule diameter causes larger high stress regions.

Table 3. Maximum normalized stress

	Vascular channel diameter			
	1 mm	0.8 mm	0.6 mm	0.4 mm
UD 0	0.0681	0.06734	0.06717	0.067
UD 90	0.5534	0.5514	0.5498	0.5498
$[0/90]_{4s}$	0.12585	0.12534	0.1247	0.1247

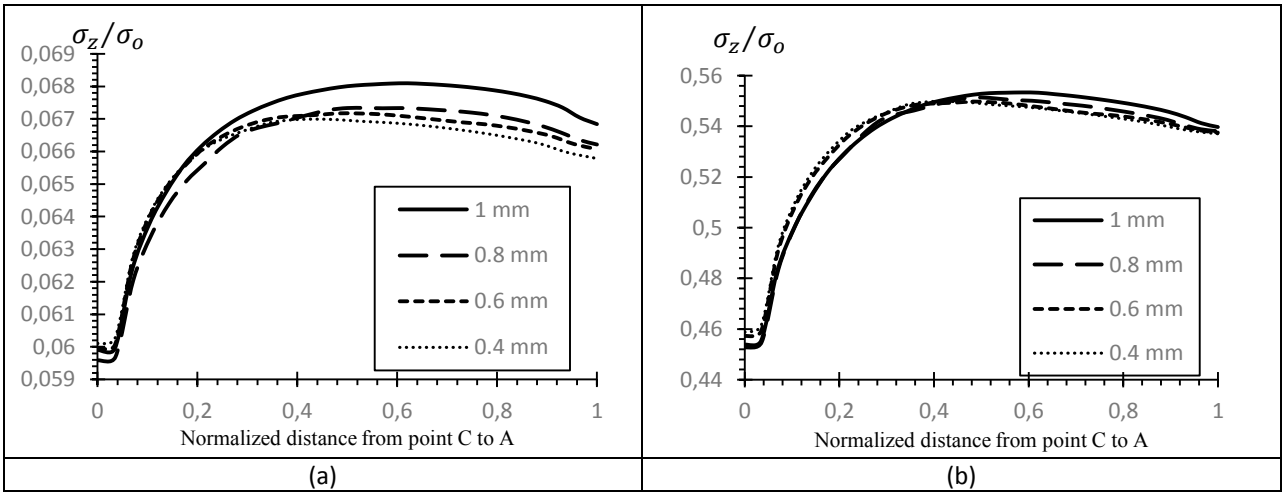

Fig. 1. Normalized σ_z distribution along C-A for different vascular diameter with stacking sequences (a) UD 0 ; (b) UD9 0

.

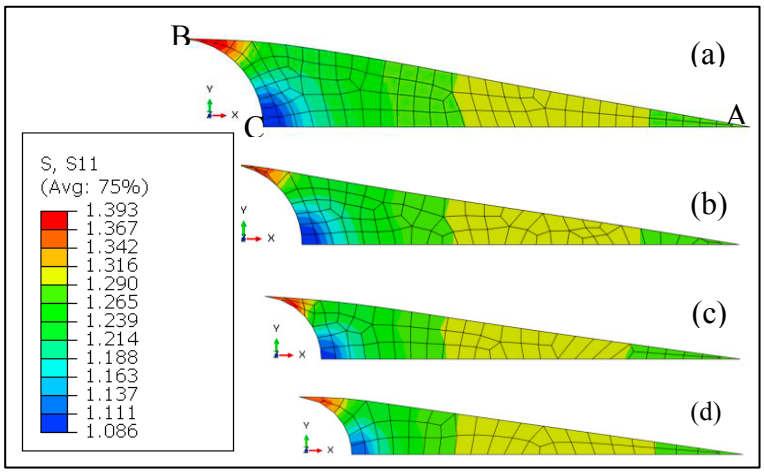

Fig. 2. Longitudinal stress for [0/90]4s stacking order for the vascule diameter of (a) 1 mm; (b) 0.8 mm; (c) 0.6 mm; (d) 0.4 mm vascule diameter

5. Conclusion

Stress concentrations and distributions are investigated for various stacking conditions and microvascular channel diameters by introducing a 3D finite element model. The proposed model is much more flexible than the models in literature in terms of boundary conditions, loading configuration, channel size and lamina stacking sequences. Although the geometry and dimensions of resin rich zone at vascularized laminates with $[0/90]_{4s}$ and $[90/0]_{4s}$ configurations are significantly different; they had almost the same attitude under tensile load in all directions. In UD 0 stacking configuration, lowest normalized stresses are observed while in UD 90, they are highest. The effect of changing vascule diameters are more effective for UD 0 plies compared to the other stacking configurations. The maximum point of stress concentrations is shifted away from the center as the diameter of the channel is increased.

Although the stress concentration results obtained in this study are small and very close to each other, it will form a basis for more advanced configurations of microvascular channels such as utilizing multiple channels and for the channels located other than between the center plies. The results obtained in this study can explain the results obtained in such advanced configurations

References

Aragón AM, Hansen CJ, Wu W, Geubelle PH, Lewis J, White SR. Computational design and optimization of a biomimetic self-healing/cooling material. Proc. SPIE Vol, vol. 6526, 2007, p. 65261G–1.

Coppola AM, Thakre PR, Sottos NR, White SR. Tensile properties and damage evolution in vascular 3D woven glass/epoxy composites. Compos Part A Appl Sci Manuf 2014;59:9–17. doi:10.1016/j.compositesa.2013.12.006.

Esser-kahn AP, Thakre PR, Dong H, Patrick JF, Vlasko-vlasov VK, Sottos NR, et al. Three-Dimensional Microvascular Fiber-Reinforced Composites 2011:3654–8. doi:10.1002/adma.201100933.

Huang C, Trask RS, Bond IP. Characterization and analysis of carbon fibre-reinforced polymer composite laminates with embedded circular vasculature. R Soc Interface 2010:1229–41.

Jensen DW, Pascual J, August JA. Performance of graphite/bismaleimide laminates with embedded optical fibers. I. Uniaxial tension. Smart Mater Struct 1992a;1:24.

Jensen DW, Pascual J, August JA. Performance of graphite/bismaleimide laminates with embedded optical fibers. II. Uniaxial compression. Smart Mater Struct 1992b;1:31.

Kousourakis a., Bannister MK, Mouritz a. P. Tensile and compressive properties of polymer laminates containing internal sensor cavities. Compos Part A Appl Sci Manuf 2008;39:1394–403. doi:10.1016/j.compositesa.2008.05.003.

Kozola BD, Shipton LA, Natrajan VK, Christensen KT, White SR. Characterization of active cooling and flow distribution in microvascular polymers. J Intell Mater Syst Struct 2010;21:1147–56.

Nguyen ATT, Orifici AC. Structural assessment of microvascular self-healing laminates using progressive damage finite element analysis. Compos Part A Appl Sci Manuf 2012;43:1886–94.

Norris CJ, Bond IP, Trask RS. The role of embedded bioinspired vasculature on damage formation in self-healing carbon fibre reinforced composites. Compos Part A Appl Sci Manuf 2011;42:639–48.

Norris CJ, Meadway GJ, O'Sullivan MJ, Bond IP, Trask RS. Self-Healing Fibre Reinforced Composites via a Bioinspired Vasculature. Adv Funct Mater 2011;21:3624–33. doi:10.1002/adfm.201101100.

Patrick JF, Hart KR, Krull BP, Diesendruck CE, Moore JS, White SR, et al. Continuous self-healing life cycle in vascularized structural composites. Adv Mater 2014;26:4302–8. doi:10.1002/adma.201400248.

Trask RS, Bond IP. Biomimetic self-healing of advanced composite structures using hollow glass fibres. Smart Mater Struct 2006;15:704.

Zhou G, Sim LM, Brewster PA, Giles AR. Through-the-thickness mechanical properties of smart quasi-isotropic carbon/epoxy laminates. Compos Part A Appl Sci Manuf 2004;35:797–815. doi:10.1016/j.compositesa.2004.01.018.